Supporting Information

$Ru(N^N)_3$-docked cationic covalent organic frameworks for enhanced sulfide and amine photooxidation

Yan-Xia Wang,[‡a] Ying Wang, [‡a] Jing Li,[b] Yang Yu,[*a] Sheng-Li Huang[*a] and Guo-Yu Yang[*a]

[b]*MOE Key Laboratory of Cluster Science, Beijing Key Laboratory of Photoelectronic/ Electrophotonic Conversion Materials, School of Chemistry and Chemical Engineering, Beijing Institute of Technology, Beijing 100081, China. E-mail: huangsl@bit.edu.cn, ygy@bit.edu.cn*

[b]*Key Laboratory of Photochemical Conversion and Optoelectronic Materials, Technical Institute of Physics and Chemistry, Chinese Academy of Sciences, Beijing 100190, China.*

Table of Contents

Table S1 Fractional atomic coordinates for the unit cell of I-COF.

References

Experimental Section

Materials

Phenylacetylene, iodomethane, tetrabutylammonium hydroxide, ruthenium(III) chloride hydrate, and 2,2'-bipyridine-4,4'-dicarboxylic acid, were purchased from Aladdin Industrial Corporation (Shanghai, China). Other reagents were purchased from Sinopharm Chemical Reagent Co., Ltd. (Shanghai, China). Chemical reagents used in this work were obtained from commercial sources and used without further purification.

Synthesis of I-COF

I-COF was synthesized using a reported protocol[1-5]. 1,3,5-Tris(4-aminophenyl)benzene (7.0 mg, 0.02 mmol), 4,4′-biphenyldicarboxaldehyde (6.3 mg, 0.03 mmol), aqueous acetate acid solution (9M, 0.07 mL), 1,4-dioxane (0.07 mL), and mesitylene (0.56 mL) were added to a Pyrex tube and mixed thoroughly by ultrasonic. The tube was flashed frozen in a liquid N_2 bath, flame sealed under a vacuum, and placed in a 120 °C oven for 72 h. After that, the solid was collected, washed with DMF and THF. Finally, the materials was dried at 80 °C under reduced pressure to give yellow colored COF-1 in an isolated yield of ~85%.

Synthesis of $[Ru(dcbpy)_3]^{4-}$

Ru(2,2'-bipyridine-4,4'-dicarboxylic acid)$_3Cl_2$ ($Ru(H_2dcbpy)_3Cl_2$) were synthesized by the reported method[6-10]. In brief, a queous solution of $RuCl_3 \cdot 3H_2O$ (50 mg, 0.19 mmol) and 2,2'-bipyridine-4,4'-dicarboxylic acid (140 mg, 0.57 mmol) was heated at 220 °C for 3 h. After cooling, the product was filtered and washed with water and methanol, and and dried under vacuum. Then, $Ru(H_2dcbpy)_3Cl_2$ was dissolved in methanol. An aqueous solution of tetrabutylammonium hydroxide was added dropwise to the solution while stirring. After stirring in half an hour, the supernatant was added to ether to obtain $[Ru(dcbpy)_3]^{4-}$.

Characterization

Instrumentation. Fourier transformed infrared spectra were recorded as KBr pellets using a Nicolet IS 10 spectrometer (FTIR: Thermo Fisher, USA). Thermo-gravimetric analysis were carried out using a DTG-60/ATG-60A thermal analyzer (TGA: Shimadzu, Japan) under a nitrogen atmosphere with a heating rate of 10 °C/min from room temperature to 1000 °C. Powder X-ray diffraction were recorded on a D8 Advance X-ray diffraction meter (PXRD: Bruker, German), using CuKα radiation over a 2θ range from 5° to 90° at a scanning rate of 3°/min. An inductively coupled plasma (ICP) spectrophotometer (Varian, 725-ES) was used to

determine Ru concentration in the catalytic solution. The N_2 adsorption-desorption isotherms were recorded at 77 K by using a BelSorp Max (Ankersmid b.v., Netherlands) surface area and porosity analyzer. Before the adsorption measurement, the samples (200 mg) were activated at 120 °C under vacuum (< 10^{-3} torr) for 12h. X-ray photoelectron spectroscopy measurement was carried out using PHI5000 Versaprobe III spectrometer (XPS: ULVAC-PHI, Japan) using an Al Kα source. The scanning electron microscope was carried out on an JSM-7500F apparatus (SEM: JEOL, Japan) equipped with a field emission gun. The UV-vis diffuse reflectance spectrawere recorded on a Nicolet Evolution 500 Spectrophotometer (UV-vis DRS: Thermo Fisher Scientific, USA ThermoFisher) with BaSO4 as reflectance standard from 200 to 900 nm.

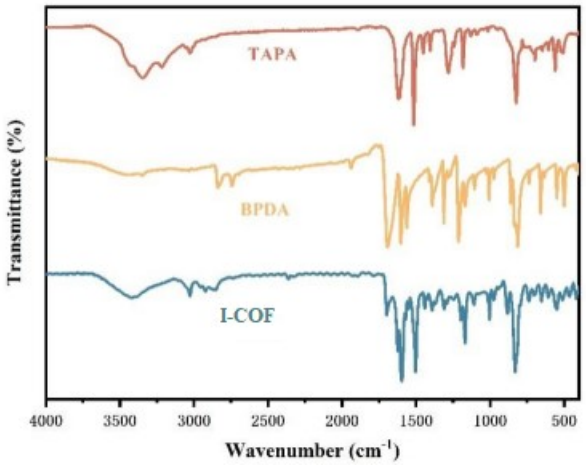

Fig. S1 FT-IR spectra for **I-COF**, 1,3,5-tris-(4-aminophenyl)benzene (TAPB) and 4,4′-biphenyldicarboxaldehyde (BPDA).

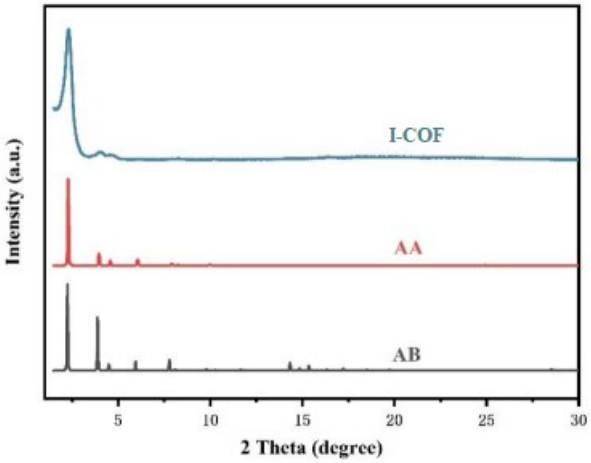

Fig. S2 PXRD patterns of **I-COF**: experimental, simulated eclipsed AA stacking, and staggered AB stacking.

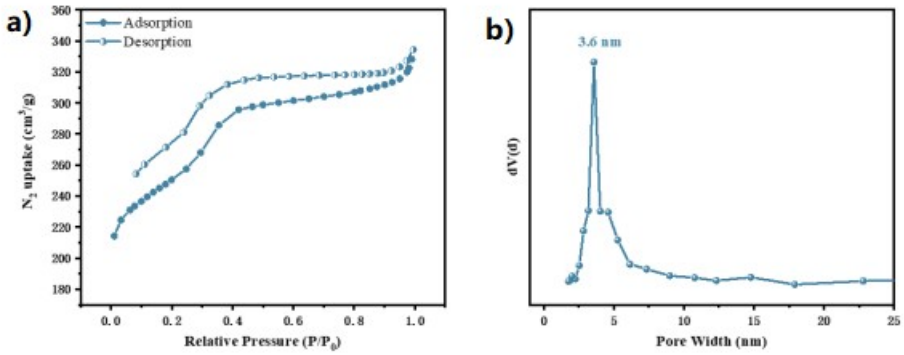

Fig. S3 (a) N_2 adsorption and desorption isotherms of **I-COF** at 77. (b) The pore size distribution of the **I-COF**.

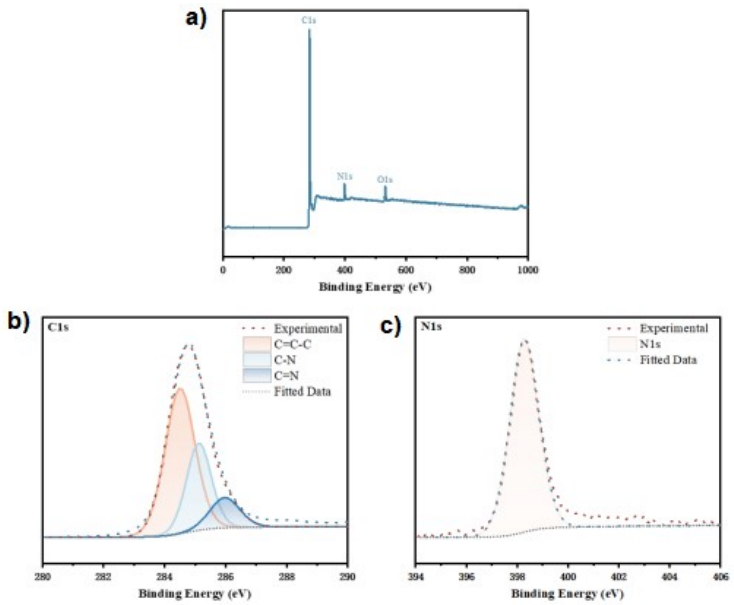

Fig. S4 (a) XPS survey data of **I-COF**. (b) C 1s and (c) N 1s deconvoluted XPS spectra of the **I-COF**.

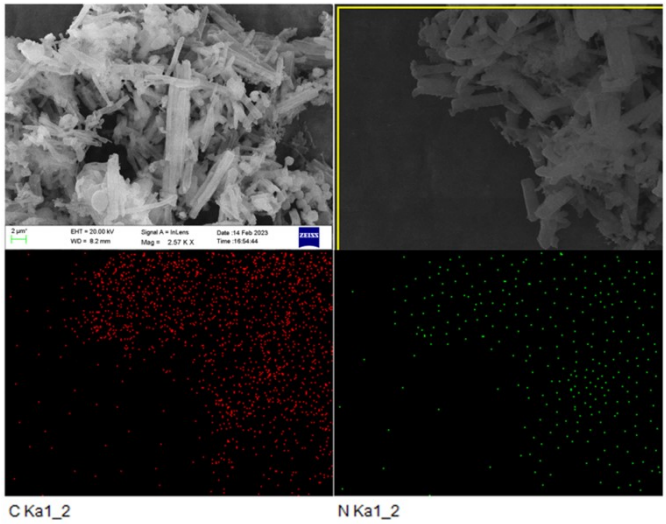

Fig. S5 SEM and EDX mapping photographs of **I-COF**.

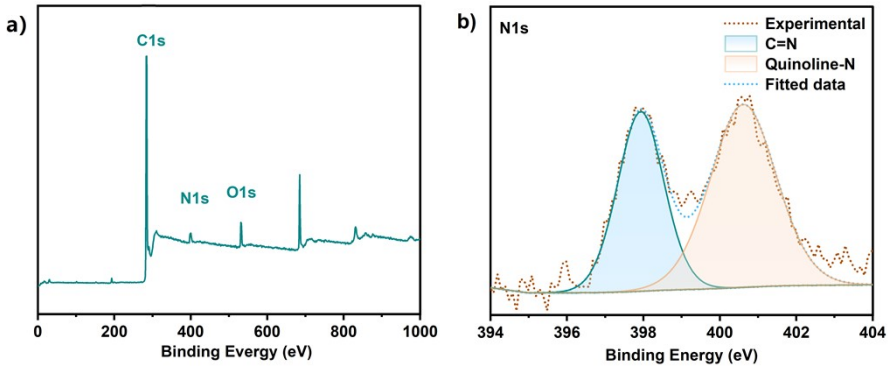

Fig. S6 (a) XPS survey data of **Q-COF**. (b) N 1s deconvoluted XPS spectra of the **Q-COF**.

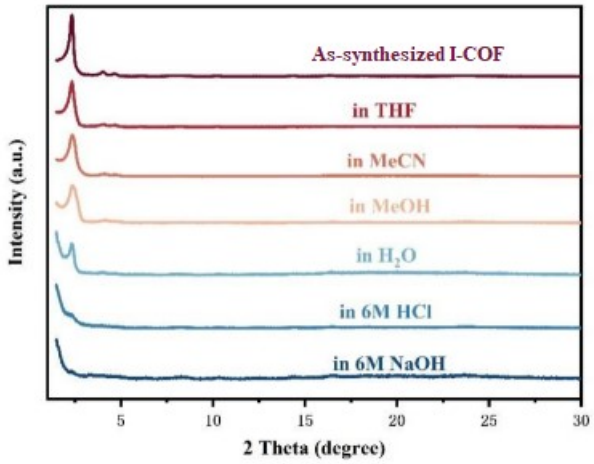

Fig. S7 PXRD patterns of **I-COF** in different experimental conditions to validate chemical stability.

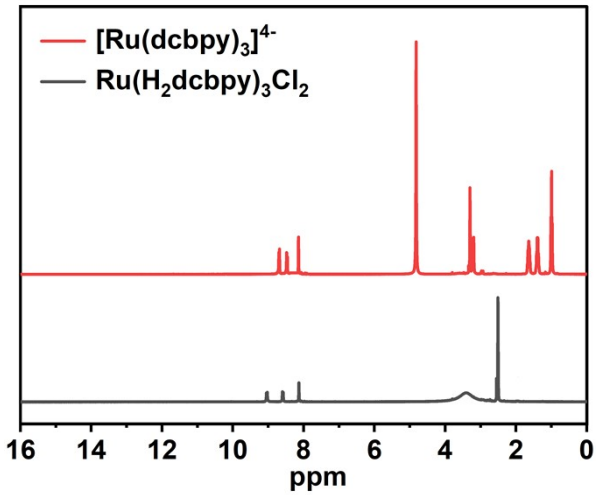

Fig. S8 ^1H NMR spectrum of $Ru(H_2dcbpy)_3Cl_2$ (DMSO-d6) and $[Ru(dcbpy)_3]^{4-}$ (CD_3OD).

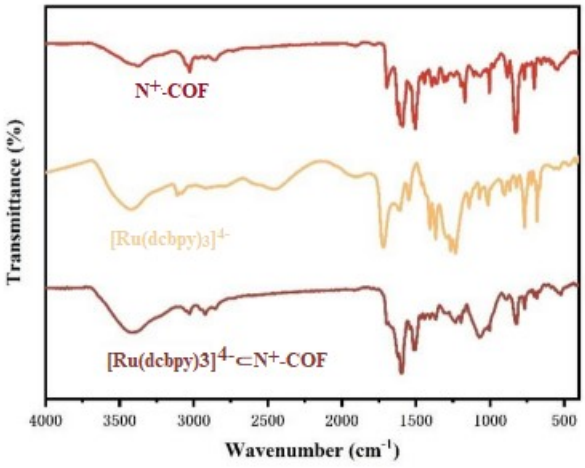

Fig. S9 FT-IR spectra for the post-synthetically modified **$[Ru(dcbpy)_3]^{4-}\subset N^+$-COF**, pristine **$N^+$-COF** and homogeneous catalyst $[Ru(dcbpy)_3]^{4-}$.

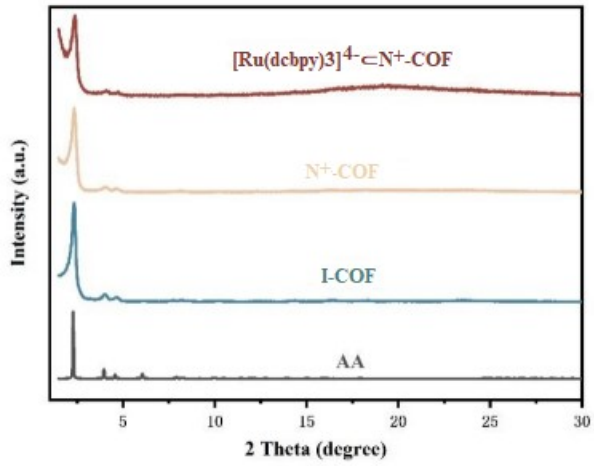

Fig. S10 PXRD patterns of **[Ru(dcbpy)$_3$]$^{4-}$⊂N$^+$-COF**, **N$^+$-COF**, **I-COF**, and simulated eclipsed AA stacking.

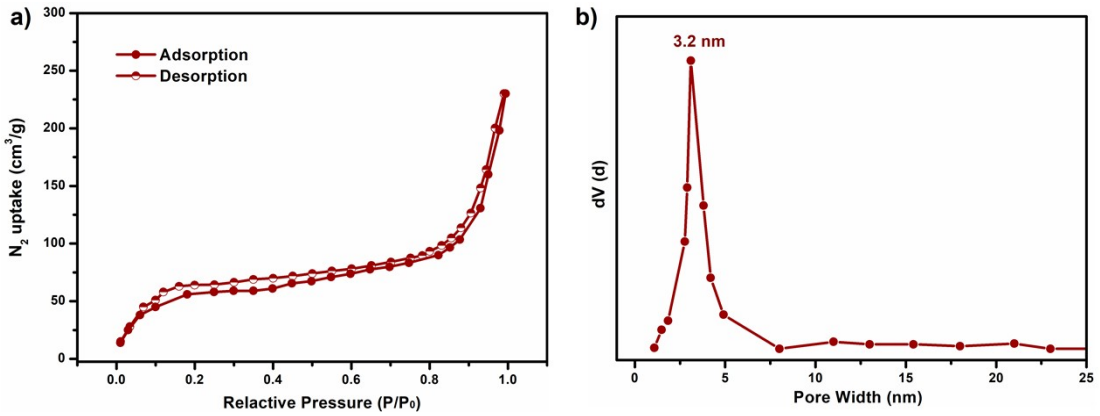

Fig. S11 (a) N_2 adsorption and desorption isotherms of **N$^+$-COF**. (b) The pore size distribution of the **N$^+$-COF**.

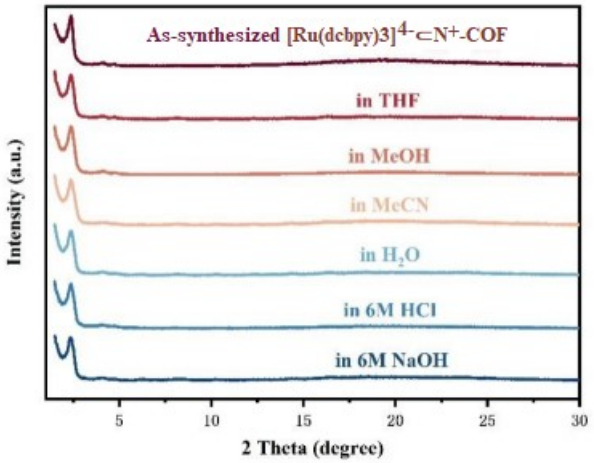

Fig. S12 PXRD patterns of **[Ru(dcbpy)$_3$]$^{4-}$⊂N$^+$-COF** in different experimental conditions to validate chemical stability.

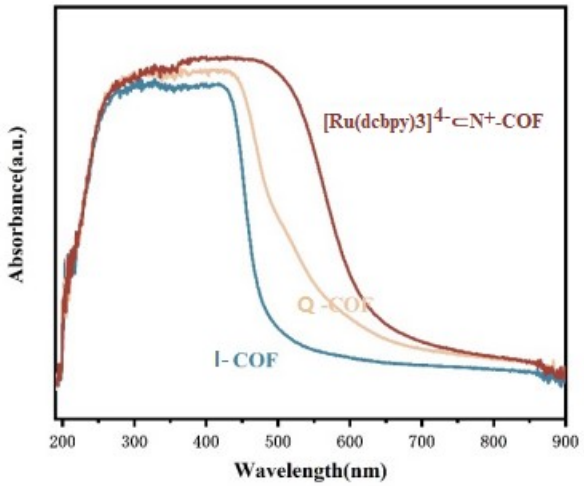

Fig. S13 Solid state UV-vis diffuse reflectance spectra of **I-COF**, **Q-COF**, and **$[Ru(dcbpy)_3]^{4-}$⊂N^+-COF**.

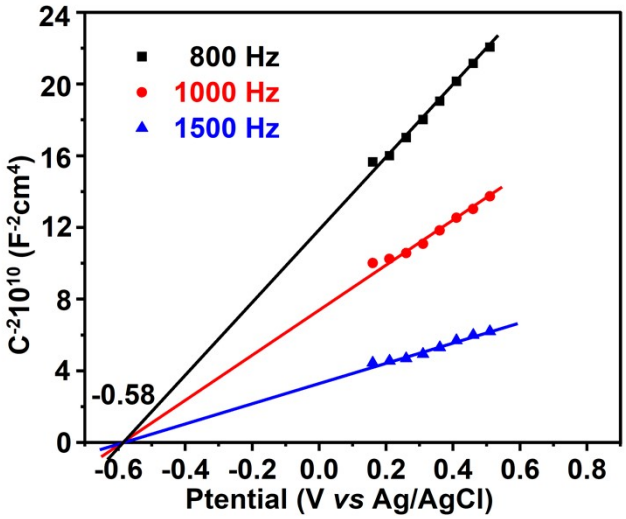

Fig. S14 Mott-Schottky plots of **N^+-COF**.

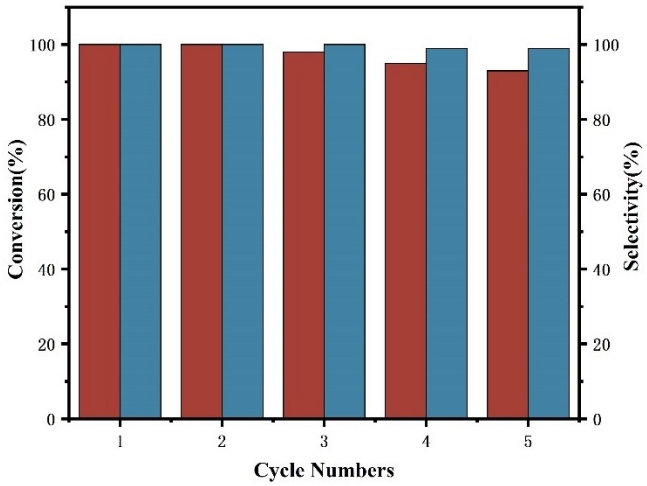

Fig. S15 Recycling experiments for photocatalytic thioanisole oxidation.

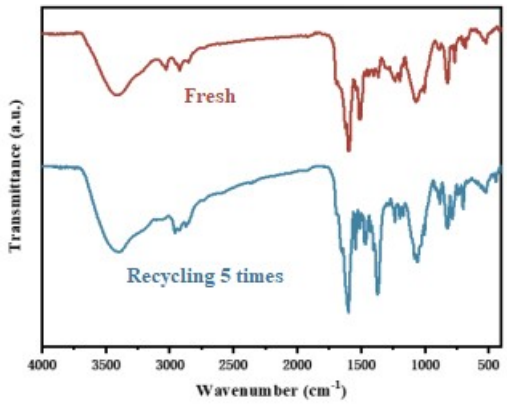

Fig. S16 FT-IR spectra of the **$[Ru(dcbpy)_3]^{4-}\subset N^+$-COF** and recycled samples of **$[Ru(dcbpy)_3]^{4-}\subset N^+$-COF** after 5 cycles of use for photocatalytic thioanisole oxidation.

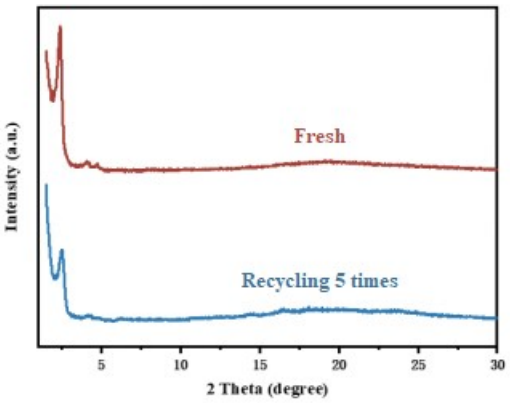

Fig. S17 PXRD patterns of the **$[Ru(dcbpy)_3]^{4-}\subset N^+$-COF** and recycled samples of **$[Ru(dcbpy)_3]^{4-}\subset N^+$-COF** after 5 cycles of use for photocatalytic thioanisole oxidation.

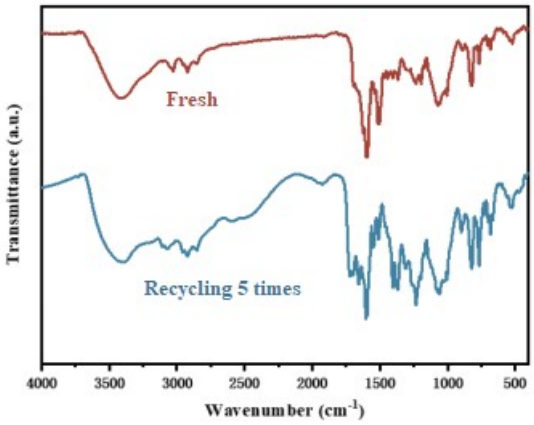

Fig. S18 FT-IR spectra of the **$[Ru(dcbpy)_3]^{4-}\subset N^+$-COF** and recycled samples of **$[Ru(dcbpy)_3]^{4-}\subset N^+$-COF** after 5 cycles of use for photocatalytic benzylamine oxidation.

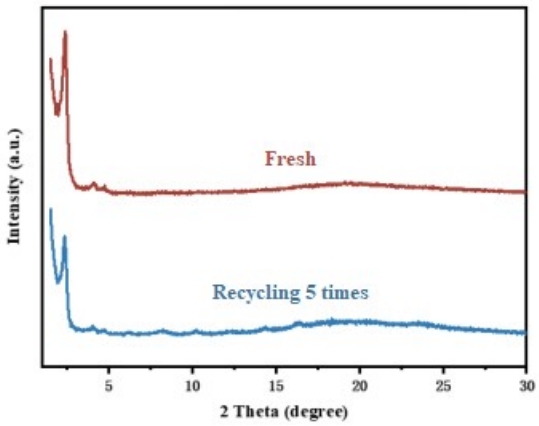

Fig. S19 PXRD patterns of the **$[Ru(dcbpy)_3]^{4-}$⊂N^+-COF** and recycled samples of **$[Ru(dcbpy)_3]^{4-}$⊂N^+-COF** after 5 cycles of use for photocatalytic benzylamine oxidation.

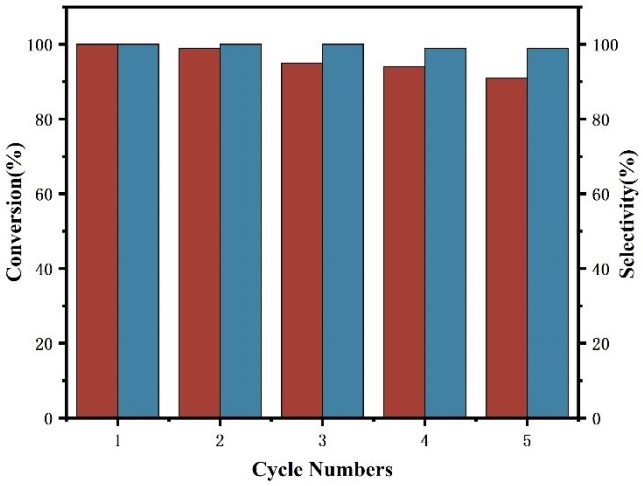

Fig. S20 Recycling experiments for photocatalytic benzylamine oxidation.

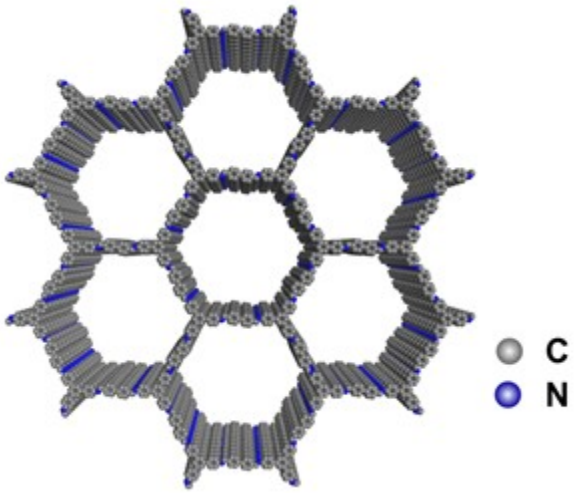

Scheme S1 Packing structures of the proposed **I-COF**.

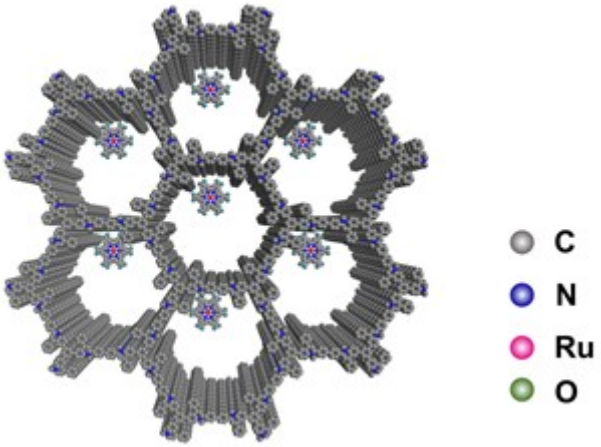

Scheme S2 Packing structures of the proposed **$[Ru(dcbpy)_3]^{4-}\subset N^+$-COF**.

Table S1 Fractional atomic coordinates for the unit cell of **I-COF**.

COF-1 (unit cell parameters: $a = b = 45.4467$Å, $c = 3.4625$Å; $\alpha = \beta = 90°$, $\gamma = 120°$)				
Label	Type symbol	*x*	*y*	*z*
C1	C	0.44198	-0.46749	0.5
C2	C	0.47711	-0.44528	0.5
C3	C	0.49964	-0.45779	0.5
C4	C	0.48781	-0.49316	0.5
C5	C	0.45211	-0.51514	0.5
C6	C	0.42972	-0.50247	0.5
C7	C	0.41782	-0.45471	0.5
N8	N	0.57128	-0.57775	0.5
C9	C	0.59142	-0.59408	0.5
C10	C	0.5745	-0.62941	0.5
C11	C	0.59239	-0.64703	0.5
C12	C	0.62846	-0.62971	0.5
C13	C	0.64516	-0.59365	0.5
C14	C	0.62703	-0.57625	0.5
C15	C	0.64818	-0.64878	0.5
C16	C	0.31597	-0.36864	0.5
H17	H	0.48717	-0.41808	0.5
H18	H	0.5262	-0.43899	0.5
H19	H	0.44056	-0.54234	0.5
H20	H	0.40262	-0.52015	0.5
H21	H	0.391	-0.47309	0.5
H22	H	0.54701	-0.64339	0.5
H23	H	0.57689	-0.67422	0.5
H24	H	0.67231	-0.57777	0.5
H25	H	0.64131	-0.54887	0.5
H26	H	0.30275	-0.39552	0.5

References

1 R. Chen, T. L. Hu and Y. Q. Li, Stable nitrogen-containing covalent organic framework as porous adsorbent for effective iodine capture from water, React. Funct. Polym., 2021, 159, 104806.

2 Y. Y. Qian, Y. L. Han, X. Y. Zhang, G. Yang, G. Z. Zhang and H. L. Jiang, Computation-based regulation of excitonic effects in donor-acceptor covalent organic frameworks for enhanced photocatalysis, Nat. Commun.,2023, 14, 3083.

3 X. Miao, F. L. Zhang, Y. X. Wang, X. Y. Dong and X. J. Lang, 2D β-ketoenamine-linked triazine covalent organic framework photocatalysis for selective oxidation of sulfides, Sustain. Energ. Fuels, 2023, 7, 1963-1973.

4 Y. Q. Li, Q. Wang, Y. H. Ju, Y. R. Li, Y. B. Zhang and R. G. Hu, Novel pyridine-based covalent organic framework containing N, N, N-chelating sites for selective detection and effective removal of nickel, Inorg. Chem. Front., 2022, 9, 3845-3853.

5 X. F. Feng, Z. Gao, L. H. Xiao, Z. Q. Lai and F. Luo, A Ni/Fe complex incorporated into a covalent organic framework as a single-site heterogeneous catalyst for efficient oxygen evolution reaction, Inorg. Chem. Front., 2020, 7, 3925-3931.

6 S. L. Huang, N. F. Liu, Y. Ling and H. K. Luo, IrIII-based octahedral metalloligands derived primitive cubic frameworks for enhanced CO_2/N_2 separation, Chem. Asian J., 2017, 12, 3110-3113.

7 G. X. Lan, Y. J. Fan, W. J. Shi, E. You, S. S. Veroneau and W. B. Lin, Biomimetic active sites on monolayered metal-organic frameworks for artificial photosynthesis, Nat. Catal., 2022, 5, 1006-1018.

8 P. Mahadevi, S. Sumathi, A. Metha and J. Singh, Synthesis, spectral, antioxidant, in vitro cytotoxicity activity and thermal analysis of schiff base metal complexes with 2, 2′-Bipyridine-4, 4′-dicarboxylic acid as co-ligand, J. Mol. Struct., 2022, 1268, 133669.

9 B. Pashaei and H. Shahroosvand, Molecularly engineered ruthenium polypyridyl complexes for using in dye-sensitized solar cell, Inorg. Chem. Commun., 2020, 112, 107737.

10 A. V. Müller, K. T. de Oliveira, G. J. Meyer and A. S. Polo, Inhibiting charge recombination in *cis*-Ru $(NCS)_2$ diimine sensitizers with aromatic substituents, ACS Appl. Mater. Interfaces, 2019, 11, 43223-43234.